Available online at www.sciencedirect.com
SCIENCE DIRECT®
ELSEVIER
Earth and Planetary Science Letters 213 (2003) 133–148
EPSL
www.elsevier.com/locate/epsl

Kinetics of convective crystal dissolution and melting, with applications to methane hydrate dissolution and dissociation in seawater☆

Youxue Zhang*, Zhengjiu Xu

Department of Geological Sciences, The University of Michigan, Ann Arbor, MI 48109-1063, USA

Received 25 February 2003; received in revised form 15 May 2003; accepted 22 May 2003

Abstract

Large quantities of methane hydrate are present in marine sediment. When methane hydrate is exposed or released to seawater, it dissolves in seawater or dissociates into methane gas and water. There was some confusion in the literature about the kinetics of these processes. It is critical to realize that dissolution and dissociation are two different processes. Dissolution is due to instability in the presence of seawater (similar to dissolution of NaCl in water) and is controlled by mass transfer. Dissociation is due to inherent instability (similar to melting of ice) with or without water (although presence of warm water may increase the dissociation rate). Dissociation of methane hydrate into gas and water is similar to ice melting and is controlled by heat transfer. Hence dissolution is relatively slow and dissociation is rapid. In this work, we extend previous theory on convective crystal dissolution and melting to greater Reynolds numbers. We carry out laboratory experiments on the dissolution and descent of NaCl, KCl, NaBr and KBr in water to verify the applicability of our theory. We then apply our models as well as previous ones to estimate methane hydrate dissolution and dissociation rates for several cases, including dissolution of exposed methane hydrate floor, dissolution and dissociation of hydrate as it rises through seawater. The results show: (i) convective dissolution rate of exposed hydrate floor is of the order 0.07 m/yr; (ii) convective dissolution rate of a rising hydrate crystal is 0.2–0.3 μm/s and a crystal of 5 mm radius is able to survive the rise through an 1800 m seawater column; and (iii) convective dissociation rate is high and depends on the difference between the ambient water temperature and the equilibrium dissociation temperature of hydrate. Starting from a depth when hydrate just reaches dissociation instability, a hydrate sphere of 5 mm radius would survive only a 47 m water column. Because hydrate is unstable in the surface ocean and would undergo rapid dissociation, only very large hydrate chunks (greater than about 0.09 m radius) would be able to survive a 530 m surface water column.

Keywords: Sherwood number; crystal dissolution; methane hydrate dissociation

* Corresponding author. Tel.: +1-734-763-0947; Fax: +1-734-763-4690.
E-mail address: youxue@umich.edu (Y. Zhang).

☆ Supplementary data associated with this article can be found at 10.1016/S0012-821X(03)00297-8.

0012-821X/03/$ – see front matter © 2003 Elsevier Science B.V. All rights reserved.
doi:10.1016/S0012-821X(03)00297-8

1. Introduction

Huge quantities of methane are stored in marine sediment in the form of methane hydrate, methane bubbles, and dissolved methane in pore water [1–3]. Various processes and conditions can lead to the release of methane hydrate into ocean water. For example, methane hydrate may be exposed onto the ocean floor, or released into seawater due to disturbance of marine sediment or oceanographic changes, such as methane bursting, landslide, faulting, or a rise in ocean bottom water temperature. Once hydrate is exposed to seawater, it becomes unstable with respect to either dissolution or dissociation. How long would an exposed layer of massive hydrate survive? How long would a piece of hydrate survive as it buoyantly rises through seawater? Would a piece of hydrate be able to survive the whole ocean column and reach the atmosphere? Would methane in hydrate dissolve in seawater or vent into the atmosphere? In this report, we investigate the kinetics and dynamics of the unstable hydrate decomposing to methane and water.

Methane can exist in the marine environment as hydrate, free gas or dissolved species in water. In order to understand the kinetics, it is necessary to first understand the stability of methane phases in the marine environment. Fig. 1 is a phase diagram of the CH_4–H_2O system at a constant temperature of 4°C (see figure caption for references). Fig. 2 is a phase diagram for the methane–seawater system constructed along a marine temperature and pressure profile, i.e., along a geotherm [4]. Because methane hydrate limits it, the solubility of CH_4 in seawater at a given depth is that corresponding to the smaller of the pressure for hydrate formation or the hydrostatic pressure (Fig. 2)[1]. For this given geotherm, hydrate is a stable phase (as long as CH_4 concentration is high) from 537 m depth to 3225 m depth (450 m below seafloor). At water depths shallower than 537 m, or at sediment depths greater than 450 m, methane hydrate is not a stable phase anymore, and would dissociate into methane and water.

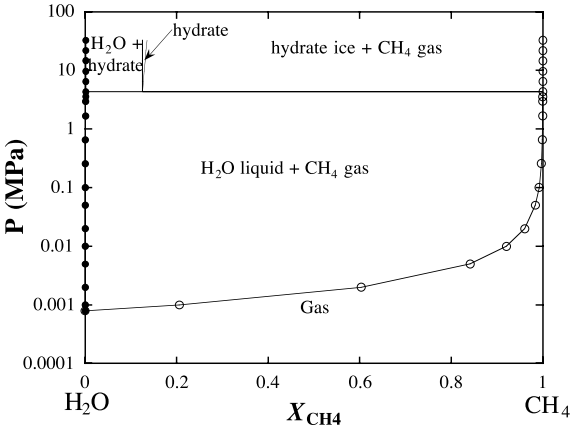

Fig. 1. A calculated phase diagram of CH_4–H_2O at 4°C. The pressure to stabilize methane hydrate is 4.31 MPa, calculated from [27]. The solubility of CH_4 in water (line connecting solid dots) as a function of P is calculated from [28] and is limited by hydrate formation above 4.31 MPa. The solubility of CH_4 in water is too low to be clearly seen (see Fig. 2 for the solubilities).

For other locations, the corresponding phase diagram can be similarly constructed and is in general different because the temperature–depth profile depends on location. For example, if the seafloor depth is only 400 m and other conditions are the same, there would be no hydrate stability field. The phase diagram along a geotherm (such as that in Fig. 2) is essential in understanding the distribution of methane hydrate and gas in sediment, as well as the kinetic processes.

To understand the kinetics of heterogeneous reactions involving methane hydrate, it is necessary to distinguish different reaction regimes because the kinetic controls are very different. The different reaction regimes are introduced here, and some terms are defined below (also along the phase boundaries in Fig. 2) for convenience of reference. Methane hydrate instability can be either by *dissolution* into water without formation of gas bubbles, or by *dissociation* into CH_4 gas phase (bubbles) and water. Dissolution occurs when methane hydrate is inherently stable at the P–T conditions (e.g., when no water is present) but is undersaturated in seawater (similar to

[1] See Appendix 1 in the online version of this paper for more comments.

NaCl or $CaSO_4 \cdot 2H_2O$ dissolution in water). Because this instability is due to the presence of an external phase (seawater), it may be called external instability. The opposite process to dissolution is methane hydrate precipitation when dissolved CH_4 concentration in water is oversaturated with respect to hydrate.

Dissociation occurs when methane hydrate is inherently unstable at the P–T conditions (similar to ice melting). (Methane hydrate dissociation into gas and ice is not similar to melting, can be slow, and will not be discussed in this work.) Dissociation does not require the presence of water, although the rate may depend on whether water is present. Because in this case the phase is unstable regardless of external phases, this instability may be called inherent instability. The opposite process is condensation of CH_4 gas and liquid water to hydrate.

The kinetic control for dissolution is mass transfer and that for dissociation is heat transfer. Because the heat transfer rate is much greater than that of mass transfer, dissociation is expected to be much more rapid than dissolution.

Both dissolution and dissociation are encountered in the ocean environment (Fig. 2). Some authors confuse dissolution and dissociation and wonder why massive gas hydrate would not sublime and dissociate when it comes into contact with deep water [5]. As shown in Fig. 2, in deep water (>537 m depth), methane hydrate is inherently stable but externally unstable, and would undergo dissolution (instead of dissociation). Because dissolution is relatively slow, massive hydrate on the ocean floor may survive for many years. On the other hand, dissociation is rapid. Hence hydrate reaching shallow water (e.g., ≤ 537 m depth in Fig. 2) is expected to disappear rapidly. Dissolution and dissociation rates will be quantified in this work. In the following sections, we first review theories of crystal dissolution and melting (dissociation) under various conditions. Then we extend previous theoretical analyses to greater Reynolds numbers. We then carry out experiments to verify our new theories. We finally apply previous and our new theories to calculate methane hydrate dissolution and dissociation rates in seawater for several cases. The behavior of methane bubbles will be discussed in a future contribution.

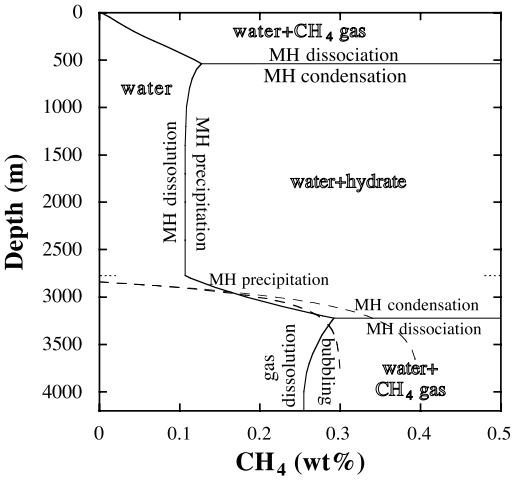

Fig. 2. A calculated phase diagram for the CH_4–seawater system in the oceanic environment. Both T and P vary with depth corresponding to water and sediment temperature and pressure along a marine geotherm [4]. Seafloor depth (at 2775 m corresponding to Blake Ridge) is marked by dotted ticks. Solid curves indicate phase boundaries. The solubility of CH_4 in seawater as a function of T and P is calculated from [28]. The stable phase assemblage in each field is shown in outline face. The phase 'water' means seawater plus dissolved CH_4. The kinetic processes across each major boundary are marked in plain text. MH = methane hydrate. The long-dashed curves show two possible profiles of total CH_4 concentration (including dissolved CH_4, CH_4 in methane hydrate, and CH_4 in gas phase) in pore water before any modification by mass transport or compaction. See [32] for actual total CH_4 concentration profile in pore water. Adapted from [4].

2. General considerations and review of crystal dissolution in liquid

Crystal dissolution in a liquid requires both mass transfer (which includes diffusive and convective mass transfer) and interface reaction [6–15]. That is, the crystal dissolution rate may be controlled by either interface reaction, or mass transfer, or a combination of the two. When mass transfer controls the dissolution rate, i.e., when mass transfer is slow and interface reaction is rapid, there is a concentration gradient in the liquid (dashed curve in Fig. 3), and the interface

liquid is roughly at equilibrium with the crystal, with very small undersaturation driving the dissolution. In this case, stirring the solution would increase the dissolution rate. When interface reaction controls the dissolution rate, i.e., when interface reaction rate is slow compared to mass transfer, the concentration gradient in the liquid is zero and the interface is undersaturated (solid horizontal line in Fig. 3). In this case, stirring the solution would not increase the dissolution rate. When both processes control the dissolution rate, the concentration profile would be between the dashed curve and the solid line in Fig. 3.

Because diffusion coefficients of different solute species in water do not vary greatly ($\sim 10^{-9}$ m^2/s [16]), whether the dissolution of a crystal in water is controlled by interface reaction or by mass transfer is primarily determined by the interface reaction rate, which is primarily controlled by bond strength of the crystal. If the bonds in the crystal are weak and hence easy to break, then interface reaction rate would be high, and dissolution would be controlled by mass transfer. If the bonds are strong and hence difficult to break, then interface reaction rate would be low and dissolution would be controlled by the interface reaction rate. Since ice melting is controlled by heat transfer (e.g., [17]), it is expected that methane hydrate dissociation is also controlled by heat transfer, and hence dissolution (which is much slower than dissociation) is controlled by mass transfer.

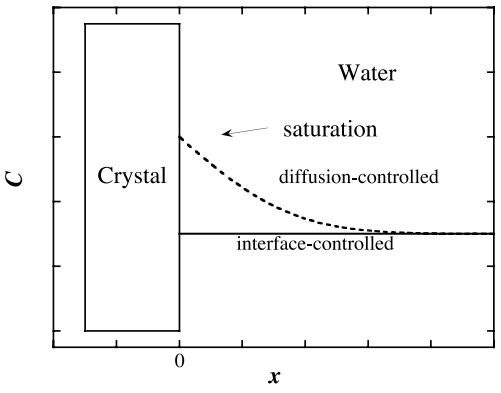

Fig. 3. Sketch of the concentration profiles during crystal dissolution controlled either by mass transfer (dashed curve, with the interface only slightly undersaturated) or by interface reaction (solid horizontal line, with constant concentration and large undersaturation at the interface). The concentration C is that of the main component in the dissolving crystal. The unit of concentration is arbitrary.

2.1. Some dimensionless numbers

Some dimensionless numbers that are necessary for the theoretical development in this paper are summarized here.

The Reynolds number (Re) is defined as:

$$\mathrm{Re} = \frac{(2a)u\rho_\mathrm{f}}{\mu} \tag{1}$$

where a is the radius of the dissolving crystal (or effective radius for a nonspherical crystal), u is the ascent or descent velocity of the crystal, ρ_f is the density of the fluid (water or seawater in this study), and μ is the viscosity of the fluid. The Notation list explains the variables and parameters.

The Rayleigh number is defined as:

$$\mathrm{Ra} = \frac{8ga^3|\Delta\rho|}{\mu D} \tag{2}$$

where g is acceleration due to Earth's gravity, $|\Delta\rho|$ is the absolute density difference between far-field liquid and the gravitationally unstable liquid at the crystal–liquid interface, and D is the diffusivity of the solute in the liquid.

The compositional Peclet number ($\mathrm{Pe_c}$), characterizing the relative importance of flow versus diffusion, is defined as:

$$\mathrm{Pe_c} = 2au/D \tag{3}$$

The thermal Peclet number ($\mathrm{Pe_t}$), characterizing the relative importance of flow versus heat conduction, is defined as:

$$\mathrm{Pe_t} = 2au/\kappa \tag{4}$$

where κ is the heat diffusivity.

The Schmidt number (Sc) is defined as:

$$\mathrm{Sc} = (\mu/\rho_\mathrm{f})/D \equiv \mathrm{Pe}/\mathrm{Re} \tag{5}$$

2.2. Dissolution rates under various conditions

Mass transfer can be accomplished by either

diffusion or convection (and advection). When mass transfer is by diffusion only (i.e., when convection is negligible), the dissolution distance can be modeled as follows [9,18]:

$$X_{\mathrm{dis}} = 2\alpha\sqrt{Dt} \tag{6}$$

where X_{dis} is the dissolution distance, t is the time, and α is solved from the following equation:

$$\sqrt{\pi}\alpha e^{\alpha^2}\mathrm{erfc}(-\alpha) = \beta_c \tag{7}$$

where erfc is the complementary error function, and β_c is defined as:

$$\beta_c = (C_{\mathrm{sat}} - C_\infty)/(C_{\mathrm{crystal}} - C_{\mathrm{sat}}) \tag{8}$$

where C_{sat} is the concentration of the solute (e.g., CH_4 for methane hydrate) at the interface liquid at saturation, C_∞ is the solute concentration in liquid far away from the crystal dissolution surface (if it is much smaller than C_{sat}, C_∞ may be taken as zero), and C_{crystal} is the solute concentration in the crystal to be dissolved; all concentrations are in mol/l.

The rate of dissolution (V) is:

$$V = -\mathrm{d}a/\mathrm{d}t = \mathrm{d}X_{\mathrm{dis}}/\mathrm{d}t = \alpha\sqrt{D/t} \tag{9}$$

where a is thickness or radius of the crystal.

In addition to diffusive dissolution, crystal dissolution may be aided by convection. Convection may arise due to various kinds of buoyancy instability (free convection, or natural convection), or due to motion of the crystal relative to the far-field liquid (forced convection) [15]. Convective dissolution of a solid floor or roof under free convection has been investigated [11]. Convective dissolution of a solid floor under forced convection due to fluid flow over it can be solved similar to heat transfer [19], leading to the following dissolution rate at high Re:

$$V = 0.03\beta_c D^{2/3} u^{4/5} (\mu/\rho_f)^{-7/15} l^{-1/5} \tag{10}$$

where l is the length scale of the system.

Convective dissolution of a crystal freely (buoyantly) rising or falling through a liquid has been investigated by Kerr [12]. His analysis is restricted to $\mathrm{Re} \leq 1$. Since Re for methane hydrate rising through seawater is often much greater than 1, we extend the theoretical analysis to $\mathrm{Re} \leq 10^5$ in Section 3. We also verify the theoretical results by experiments.

Mathematically, melting can be treated in a similar fashion as dissolution except that mass transfer is replaced by heat transfer (including replacement of δ_c by δ_t, Pe_c by Pe_t, Sherwood number by Nusselt number, etc.). Kerr [10] and McLeod and Sparks [20] investigated convective melting of a falling or rising solid sphere in a fluid for $\mathrm{Re} \leq 1$. We also extend the analysis to $\mathrm{Re} \leq 10^5$. Since both melting and dissociation are controlled by heat transfer, we will use the theory for melting to treat hydrate dissociation.

3. Convective dissolution of a crystal rising or falling in water

For convective dissolution of a crystal as it buoyantly rises or falls through water, mass transfer is enhanced and typically dominated by forced convection due to buoyant descent or ascent of a crystal. The motion of the crystal induces a flow field, and the flow removes the liquid next to the crystal, resulting in a thin compositional boundary layer next to the dissolving crystal. The boundary layer thickness is thin on the leading side of the crystal and thick on the trailing side [21]. Although the thickness of the boundary layer is variable on different sides of the moving crystal, an average boundary layer thickness (δ_c) is defined to characterize the average mass flux through the layer:

$$\delta_c = D\Delta C/F_c \tag{11}$$

where $\Delta C = C_{\mathrm{sat}} - C_\infty$ is the solute concentration difference between the interface liquid and far-away liquid, and F_c is the compositional flux from the dissolving crystal.

Using this definition, convective dissolution rate can be modeled as [9,12]:

$$-\mathrm{d}a/\mathrm{d}t = \beta_c D/\delta_c \tag{12}$$

Diffusive crystal dissolution may also be treated using the concept of boundary layer thickness. By comparing Eqs. 9 and 12, it can be seen that

diffusive crystal dissolution can be treated by Eq. 12 with a time-dependent boundary layer thickness:

$$\delta_{c,dif} = \frac{\beta_c}{\alpha}\sqrt{Dt} \quad (13)$$

From Eq. 12, if D has been measured and β_c can be estimated[1], the problem of obtaining the dissolution rate becomes the problem of obtaining the average boundary layer thickness δ_c. As outlined by Kerr [12], for forced convection, δ_c can be estimated from the Sherwood number (Sh), which in turn can be estimated from Pe_c. Sh is defined to be the ratio of the compositional flux (F_c) from the dissolving crystal to the mass flux scale:

$$Sh = \frac{F_c}{D\Delta C/(2a)} \quad (14)$$

Combining Eqs. 11 and 14, Sh can be written as:

$$Sh = 2a/\delta_c \quad (15)$$

Kerr [12] developed the theory for convective crystal dissolution in which both the crystal ascent/descent velocity and Sh are obtained using relations applicable only for $Re \leq 1$. In this section, we extend the analyses to cover $Re \leq 10^5$. Below, we first develop a unifying relation for the dependence of Sh on Pe_c and Re. We then present the analyses of convective crystal dissolution at both low and high Re. We then present laboratory experimental data to verify the theoretical analyses. Methane hydrate dissolution upon buoyant ascent in seawater will be modeled in Section 3.3.

3.1. A simple unifying expression for Sh for forced convection

We first develop a simple expression for Sh for a large range of Re to simplify the theory for convective crystal dissolution. The expressions of Sh under various conditions have been parameterized by Clift et al. [22] as follows:

For $Re<1$, $Sh = 1 + (1 + Pe_c)^{1/3}$ (16a)

For $1 \leq Re \leq 100$, $Sh = 1 + ZRe^{0.41}$ (16b)

For $100 \leq Re \leq 2000$, $Sh = 1 + 0.752ZRe^{0.472}$ (16c)

For $2000 \leq Re \leq 100000$,

$$Sh = 1 + Z(0.44Re^{0.5} + 0.034Re^{0.71}) \quad (16d)$$

where $Z = [(1+1/Pe_c)Sc]^{1/3}$. Eq. 16a is accurate to within 3% when $Re \leq 1$ and is the equation used by Kerr [12]. Eqs. 16b, 16c and 16d fit the experimental data (from different laboratories) well but the data themselves show substantial scatter [22].

The above four expressions for Sh are complicated and we simplify them below. The first step is to eliminate Sc in Z. Because $Sc = Pe/Re$, $Z = [(1+1/Pe_c)Sc]^{1/3} = [(1+Pe_c)/Re]^{1/3}$, Eqs. 16a, 16b, 16c and 16d can be rewritten as:

For $Re<1$, $Sh = 1 + (1 + Pe_c)^{1/3}$ (17a)

For $1 \leq Re \leq 100$,

$$Sh = 1 + (1 + Pe_c)^{1/3}Re^{0.41-1/3} \quad (17b)$$

For $100 \leq Re \leq 2000$,

$$Sh = 1 + (1 + Pe_c)^{1/3}0.752Re^{0.472-1/3} \quad (17c)$$

For $2000 \leq Re \leq 100000$, $Sh = 1+$

$$(1 + Pe_c)^{1/3}(0.44Re^{0.5-1/3} + 0.034Re^{0.71-1/3}) \quad (17d)$$

The second step is to use one expression to represent the above four equations in their respective applicable range. After many trials, the above four equations can be combined as:

$$Sh = 1 + (1 + Pe_c)^{1/3}\left(1 + \frac{0.096Re^{1/3}}{1 + 7Re^{-2}}\right) \quad (18)$$

Eq. 18 reproduces Eqs. 16a, 16b, 16c and 16d in their respective range to within 3%. Hence it is an excellent expression of Sh for $Re \leq 10^5$ and is recommended for future use.

3.2. Convective dissolution rate upon crystal ascent or descent in a large range of Re

For $Re > 1$, crystal ascent or descent velocity can no longer be calculated from Stokes' law, and the expression of Sh using Eq. 16a must be

replaced by Eq. 18. The following is an outline of our new model extending the model of Kerr [12]:

1. Given the radius of the crystal, calculate the ascent or descent velocity u. For Stokes flow ($Re < 1$), $u = 2ga^2\Delta\rho/(9\mu)$. If $Re > 1$, the Stokes law is no longer applicable; a more complicated formulation must be used. For $Re \leq 3\times10^5$, one formulation is to solve the three unknowns (u, Re, drag coefficient C_D) iteratively from Eq. 1 and the following two equations:

$$C_D = \frac{24}{Re}(1 + 0.15Re^{0.687}) + \frac{0.42}{1 + 42500Re^{-1.16}} \quad (19)$$

$$u = \sqrt{\frac{8ga\Delta\rho}{3\rho_{water}C_D}}. \quad (20)$$

Eq. 19 is from Cliff et al. [22] and the relative error is +6% to −4% for $Re < 3\times10^5$; Eq. 20 is from the definition of C_D and can be found in fluid dynamics books (e.g., eq. 6-230 in [23]). In the above formulation, the effect of denser interface fluid on descent velocity is ignored.

2. Knowing u from above, Pe_c can be calculated using Eq. 3. With Re (from Eq. 1) and Pe_c, Sh for forced convection can be calculated from Eq. 18.
   As shown by Kerr [12], for very tiny crystals (usually < 0.05 mm radius), free convection may be more important than forced convection. Sh for free convection is expressed as [12]:

$$Sh = 2 + 0.6Ra^{1/4} \quad (21)$$

   where Ra is the Rayleigh number (Eq. 2). The above equation applies for $Ra \leq 10^{10}$. For calculation of convective crystal dissolution rate, we calculate Sh for free convection and Sh for forced convection, and the greater value is used as Sh of the process. Only for very tiny crystals is Sh for free convection greater than that for forced convection and hence used in the calculation.
3. The value of δ_c is calculated from $\delta_c = (2a)/Sh$ (Eq. 15).
4. Then, the right-hand side of Eq. 12 is obtained, and a is solved from the differential equation (Eq. 12). Depth is solved by integrating u with respect to t, $\int u dt$.

Because of the interdependence of a, u, Re, Pe_c, Sh, and δ_c, the differential equation (Eq. 12) can only be integrated numerically. The integration is carried out with a spreadsheet program.

Because we have extended the analyses of Kerr [12] from small Re ($Re \leq 1$) to a large range of Re ($Re \leq 10^5$), and because there are some simplifying assumptions and approximate equations, below we report laboratory experiments to verify the calculated results and assess the applicability of the model.

3.3. Experimental data on convective crystal dissolution to high Re

We carried out convective dissolution experiments in water using NaCl, KCl, NaBr, and KBr crystals. The experimental apparatus consists of a glass cylinder 1.5 m long and 0.10 m in inner diameter. The experimental procedure follows that of Walker and Kiefer [8]. The experimental temperature (water temperature in the apparatus) is controlled by setting the room temperature to be either 17, 21 or 25°C, and waiting for ≥ 24 h until measured water temperature in the cylinder reaches the room temperature. Crystals that are close to cubic and appear to be free of cracks and inclusions (but inspection is difficult due to surface pits) are used for experiments. We use cubic crystals (rather than prepare them into spheres) to assess the accuracy of the spherical model on cubic crystals because hydrate crystals are our focus and they are not spherical. A cubic crystal is weighed with a microbalance. From the mass an effective radius (a) of equal volume is calculated. The crystal is dropped into water and is watched as it descends and dissolves. The duration from the moment the crystal is dropped into water until it disappears in water is recorded as the surviving time (t_s). The total vertical distance that the crystal travels in water is recorded as the surviving distance (h_s). Because we require the crystal to be completely dissolved before it reaches the bottom and because the height of the water column is

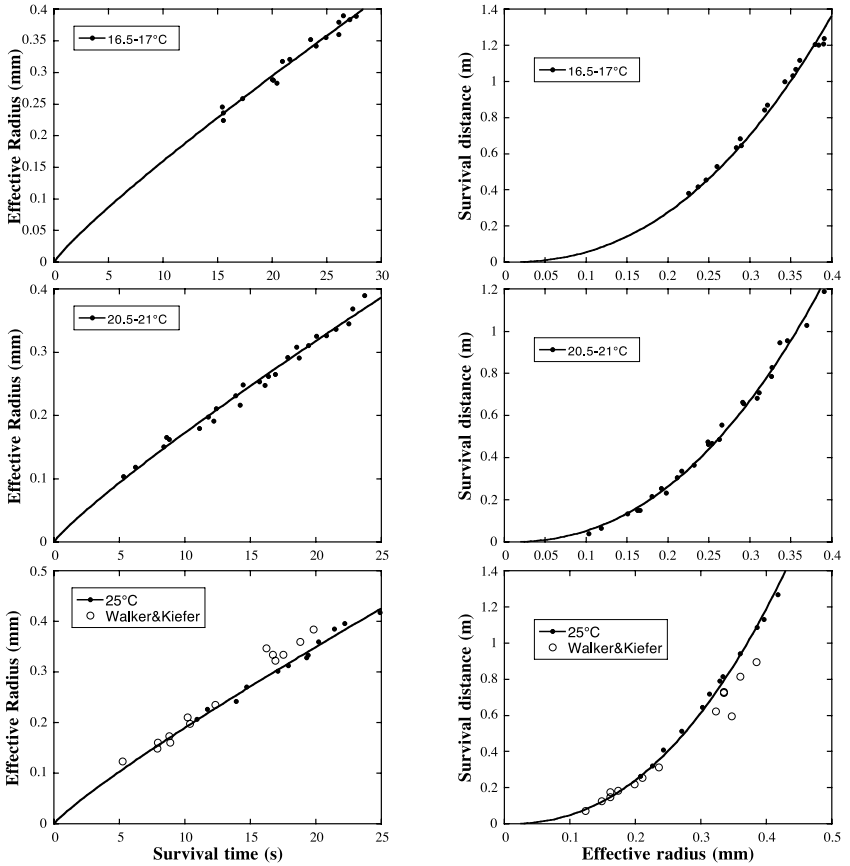

Fig. 4. Experimental convective crystal dissolution data for NaCl at three temperatures. The curves are best fit to the data (not calculated from theory). The function to fit a (mm) vs. t (s) is: $a=\gamma t^{0.88}$ where $\gamma=0.0211$ at 16.5–17°C, 0.0228 at 20.5–21°C, and 0.0251 at 25°C. The function for h vs. a is $h=\varepsilon a^{2.3}$ where $\varepsilon=11.3$ at 16.5–17°C, 10.7 at 20.5–21°C, and 9.8 at 25°C. The simple expressions of the fit functions are obtained from model calculations and are not general (they are only applicable to the data range shown in the figure).

limited, the maximum Re number of the experiments is limited to ≤ 350.

Some experiments were classified to be unsuccessful and discarded. (i) For a couple of experiments, a floating bubble appeared (presumably from a bubble inclusion in the crystal) as the crystal was dissolved. The results of these experiments were discarded. (ii) The larger the crystal, the more sideways wiggling there is as it falls down. We discarded the results if the crystal came very close (within a few mm by the naked eye) to the glass wall of the apparatus during its descent.

The uncertainty for the crystal mass is 0.002 mg, that for the surviving time is 0.2 s (larger than the reading accuracy to account for human response time), and that for the surviving distance is 0.001 m. The scatter of the data in figures is greater than these uncertainties due to other experimental uncertainties, such as deviation from cubic shape, imperfection of a crystal (e.g., inclusions and cracks), etc.

All experimental data are listed in Table 1. Some data are shown in Figs. 4 and 5. Fig. 4 shows all experimental data on NaCl, as well as fits to the data. It also compares experimental data of Walker and Kiefer [8] with our data. The agreement between the two data sets is very good. The slightly larger scatter in the data of Walker and Kiefer [8] can be attributed to the

Table 1
Experimental data for convective crystal dissolution

M mg	t_s s	h_s m	M mg	t_s s	h_s m	M mg	t_s s	h_s m	M mg	t_s s	h_s m
NaCl (16.5–17°C)			KCl (21°C)			NaBr (17°C)			KBr (21°C)		
0.103	15.5	0.383	0.043	7.06	0.117	0.309	8.3	0.420	0.085	4.29	0.139
0.120	15.5	0.418	0.061	7.47	0.137	0.342	8.5	0.435	0.135	5.50	0.189
0.135	15.4	0.455	0.083	8.84	0.194	0.429	9.5	0.540	0.253	6.84	0.2785
0.158	17.3	0.530	0.115	10.1	0.251	0.454	9.9	0.567	0.357	7.72	0.362
0.206	20.4	0.635	0.121	10.47	0.270	0.648	10.5	0.720	0.417	7.96	0.3785
0.217	20.1	0.684	0.160	11.35	0.310	0.723	11.3	0.791	0.641	8.91	0.5585
0.219	20.0	0.645	0.207	12.15	0.385	0.821	11.8	0.854	0.755	9.35	0.6585
0.291	20.9	0.844	0.272	13.44	0.465	1.025	12.7	1.000	0.863	9.65	0.675
0.301	21.6	0.871	0.291	13.81	0.498	1.092	13.5	1.008	0.996	10.75	0.779
0.364	24.0	0.999	0.340	14.85	0.516	1.225	14.0	1.125	1.343	12.12	0.9685
0.397	23.5	1.033	0.386	15.06	0.546	1.426	14.6	1.245	1.700	12.5	1.0535
0.409	24.9	1.070	0.420	15.88	0.630	NaBr (21°C)			1.785	12.62	1.0985
0.426	26.1	1.119	0.490	16.32	0.655	0.112	6.1	0.198	KBr (25°C)		
0.496	26.1	1.205	0.519	16.93	0.706	0.622	9.7	0.660	0.135	4.75	0.183
0.513	27.1	1.204	KCl (25°C)			0.702	10.0	0.711	0.208	5.84	0.227
0.537	27.7	1.210	0.047	6.75	0.120	0.920	11.2	0.870	0.311	6.91	0.313
0.540	26.5	1.239	0.053	6.44	0.131	1.264	12.8	1.087	0.600	7.60	0.510
NaCl (21°C)			0.076	8.19	0.179	1.294	12.5	1.067	0.603	7.69	0.440
0.031	8.40	0.133	0.100	8.62	0.197	NaBr (25°C)			0.603	7.78	0.453
0.053	11.1	0.216	0.110	9.31	0.215	0.082	4.6	0.153	0.790	8.40	0.596
0.064	12.2	0.253	0.122	9.56	0.241	0.097	4.7	0.1615	0.887	9.47	0.675
0.092	14.2	0.338	0.134	9.69	0.259	0.116	5.1	0.1815	0.997	9.59	0.749
0.139	16.1	0.476	0.164	9.50	0.282	0.161	5.7	0.2435	1.245	10.50	0.803
0.170	16.9	0.556	0.176	9.90	0.313	0.262	6.3	0.3255	1.639	11.41	0.980
0.224	18.7	0.665	0.200	10.38	0.340	0.345	6.9	0.4035			
0.316	20.8	0.829	0.264	11.88	0.447	0.430	8.0	0.4715			
0.373	22.5	0.955	0.335	13.22	0.517	0.505	8.3	0.5275	NaCl (20.5°C)		
0.457	22.8	1.059	0.373	12.84	0.509	0.738	9.5	0.6795	0.010	5.32	0.041
0.539	23.7	1.190	0.380	13.66	0.536	0.967	10.4	0.8215	0.015	6.22	0.067
NaCl (25°C)			0.410	13.72	0.557	1.122	11.1	0.933	0.039	8.78	0.151
0.081	10.9	0.263				1.181	11.7	0.923	0.041	8.62	0.151
0.105	11.7	0.321				1.216	11.2	0.902	0.070	11.78	0.234
0.130	13.9	0.408				1.446	12.0	1.0635	0.085	12.41	0.306
0.180	14.7	0.514				1.479	12.3	1.1035	0.113	13.87	0.366
0.251	17.1	0.646				1.719	12.6	1.2115	0.140	14.43	0.463
0.279	17.9	0.721				1.950	13.2	1.2715	0.148	15.69	0.469
0.322	19.3	0.791				2.035	13.5	1.3635	0.164	16.36	0.487
0.336	19.4	0.816							0.226	17.86	0.656
0.423	20.2	0.943							0.266	18.53	0.683
0.521	21.4	1.089							0.273	19.43	0.710
0.563	22.2	1.133							0.314	20.03	0.786
0.661	24.9	1.270							0.346	21.53	0.949

Crystals are cubic. M is the mass of the crystal; t_s is the survival time, and h_s is the survival distance. Note that experimental data for NaCl dissolution at 20.5°C are shown in the last three columns. The uncertainty in temperature is less than 0.5°C. The uncertainty in the mass is 0.002 mg. The estimated uncertainty for the survival time from a digital stopwatch is 0.2 s. The uncertainty in the survival distance is 0.001 m. In plots, the effective radius (a) is used instead of the mass and is calculated from the mass and density of the crystal using $a = [3M/(4\pi\rho)]^{1/3}$.

unairconditioned July temperature (~30°C) in their laboratory.

Experimental data and calculated results (see Fig. 5) show that the effective radius (a) and the surviving time (t_s) are roughly (but not exactly) proportional to each other over the experimental conditions of this study. To extend the results to zero crystal size, a better form is $a = kt_s^{0.88}$ where k is a constant (see fits in Fig. 4). To extend to greater crystal size, a is roughly linear to t_s. To cover both small and large crystal sizes, the following two-parameter equation, $a = k_1 t_s^{1/2} + k_2 t_s$, fits the calculated results very well. For the relation between a and the surviving distance (h_s), a rough relation is that h_s is proportional to a^2. To extend to zero crystal size, a better form is $h_s = qa^{2.3}$ where q is a constant (see fits in Fig. 4). To extend to greater crystal size, h_s is roughly linear to a^2. To cover both small and large crystal sizes, the following two-parameter equation, $a = q_1 h_s^{1/5} + q_2 h_s^{1/2}$, fits calculated results very well.

Although the above two-parameter fitting functions can fit our a vs. t_s data and a vs. h_s data very well, we still primarily focus on the comparison between our model calculation and experimental data because there is no free parameter in the model calculation.

Fig. 5 compares all experimental data at 25°C with calculation using our model developed in Section 3.2. The constants necessary for the calculations are summarized in Appendix 2[2]. For KCl, the calculated a vs. t_s curve and h_s vs. a curve are in good agreement with experimental data. For NaBr, the calculated a vs. t_s curve is in agreement with data, but the calculated h_s vs. a curve is above the data by up to 25% relative. For NaCl, the calculated a vs. t_s curve is above the data by up to 20% relative, and the calculated h_s vs. a curve is below the data by up to 15% relative. For KBr, the calculated a vs. t_s and h_s vs. a curves are both above the data by up to 20% relative.

Because there are no fitting parameters at all, this level of agreement for $Re \leq 350$ and for several types of crystals is good and implies that our model for crystal dissolution and descent captures the main controlling factors. Possible causes for the small disagreements include (in order of decreasing importance):

1. Some minor factors are ignored. Near the dissolving interface, the solute concentration is very high, and the effects on viscosity, density and diffusivity can be significant. There is also a minor thermal effect due to heat of solution. The effect of solute concentration on the diffusivity is small and complicated for these halides (usually first decreases and then increases with concentration). Viscosity of salt-bearing water strongly increases with NaCl and NaBr concentration (by about a factor of 2), but only depends weakly on KCl and KBr concentration (Appendix 2[2]). The density of halide-saturated water is greater than that of pure water by 199 kg/m^3 for NaCl, 176 kg/m^3 for KCl, 533 kg/m^3 for NaBr, and 380 kg/m^3 for KBr (Appendix 2[2]). A high viscosity would reduce the descent velocity, whereas a dense boundary layer would increase it, affecting the surviving distance. A change in the descent velocity would in turn affect Re, Sh, δ_c, and the dissolution rate.
   It appears that among the factors not incorporated into our model, viscosity and density variations in the boundary layer are the most important. For KCl, both effects are small, and calculations agree well with experimental results. For NaBr, the two effects (higher viscosity and higher density) tend to cancel each other. For NaCl, the viscosity effect dominates. For KBr, the density effect dominates. Incorporating the viscosity and density effects is difficult because they vary across the boundary layer. Hence we recognize the problems but choose to tolerate them.
2. Both Eqs. 18 and 19 have some uncertainties. Expressions for other parameters used in the calculations, such as diffusivity and solubility, also have small uncertainties. These uncertainties may lead to 10% relative uncertainties in the calculation.
3. The shape of crystals used for experiments is roughly cubic and some are prolate, whereas the calculation is done for spherical geometry.

[2] For Appendix 2 see the online version of this paper.

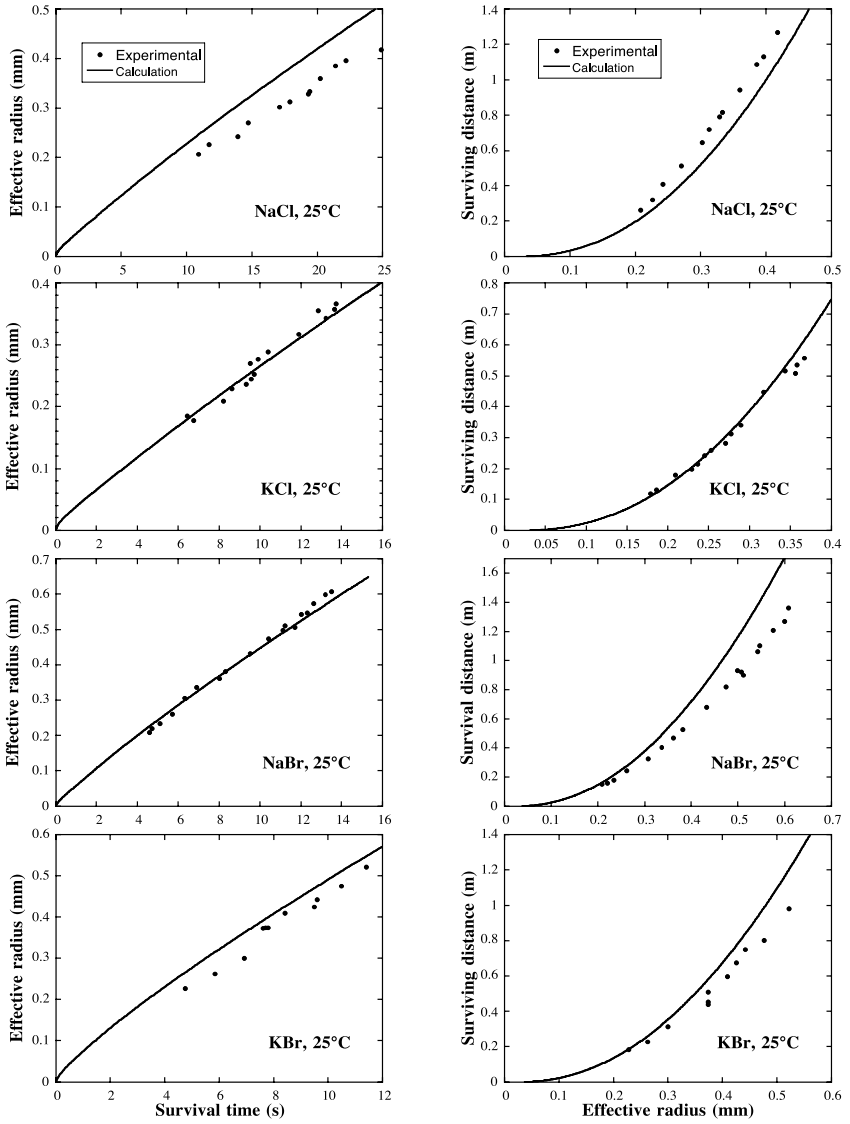

Fig. 5. Comparison of experimental data and calculated results on convective crystal dissolution. Note the curves are calculated (see Section 3.2) without any fitting parameters.

Because the theory is general to high Re number, and because there is good agreement between experimental data and theoretical calculation, we expect the theory to be approximately applicable to Re up to 10^5. In Section 5.2, we apply the theory to calculate convective dissolution rate of methane hydrate upon free ascent in seawater.

4. Convective dissociation of a crystal rising or falling in water

In the regime of methane hydrate dissociation (e.g., at water depth less than 530 m in Fig. 2), the controlling factor is heat transfer instead of mass transfer. Kinetics of methane hydrate dissociation is expected to be similar to that of ice melting

except for the generation of bubbles whose buoyant rise from the interface may enhance convection. Hence we use the theory for convective melting to approximate the theory for dissociation, but noting that the theory may only give a minimum dissociation rate.

Theory for crystal melting under forced convection as a crystal is falling or rising through a liquid can be developed by analogy with that for crystal dissolution under forced convection [12]. For $\mathrm{Re} < 1$, the theory of convective melting has been developed by Kerr [10] and McLeod and Sparks [20]. Following Section 3.3 on convective dissolution, we extend the analysis of convective dissociation (or melting) to Re number up to 10^5.

As a crystal melts, the necessary thermal flux is [10,20]:

$$F_t = (-\mathrm{d}a/\mathrm{d}t)[\rho_s c_s(T_0 - T_s) + \rho_s L] \tag{22}$$

where $(-\mathrm{d}a/\mathrm{d}t)$ is the melting rate, subscript 's' means the solid phase, c is heat capacity, L is the latent heat for crystal melting or dissociation, T_0 is the interface temperature (assumed to be the equilibrium melting or dissociation temperature [17]), T_s is the temperature inside the crystal far away from the interface. This heat must be conducted to the melting surface from the fluid. That is:

$$F_t = -k(\partial T/\partial r)_{r=a+} = -k(T_\infty - T_0)/\delta_t \tag{23}$$

where k is heat conductivity of the liquid, T_∞ is temperature in far-away liquid, and δ_t is the average thickness of the thermal boundary layer around the melting crystal. (Similar to the compositional boundary layer thickness, the thermal boundary layer thickness is also thin on the leading side of the sphere and thick on the trailing side of the sphere.) The above equation defines δ_t. Combining Eqs. 22 and 23 leads to:

$$-\mathrm{d}a/\mathrm{d}t = \beta_t \kappa/\delta_t \tag{24}$$

where κ is heat diffusivity in the liquid and equals $k/(\rho_f c_f)$, and the dimensionless parameter β_t is defined as:

$$\beta_t = \frac{\rho_f c_f (T_\infty - T_0)}{\rho_s c_s (T_0 - T_s) + \rho_s L} \tag{25}$$

where subscript 'f' means the liquid. The parameter β_t can be identified to be St^{-1} where St is the Stephan number. Since L is usually large, the denominator in the above equation can usually be approximated by $\rho_s L$. Similarity between Eqs. 12 and 24 is obvious.

To find δ_t, one uses dimensionless relations through the Nusselt number. The Nusselt number (Nu) is defined to be the ratio of the total thermal flux (F_t) from the dissolving crystal to the heat flux scale $k(T_\infty - T_0)/(2a)$:

$$\mathrm{Nu} = \frac{F_t}{k(T_\infty - T_0)/(2a)} \tag{26}$$

Combining Eqs. 23 and 26 leads to:

$$\mathrm{Nu} = 2a/\delta_t \tag{27}$$

which is similar to Eq. 15. By analogy to the relation between Sh, $\mathrm{Pe_c}$, and Re (Eq. 18), for $\mathrm{Re} \le 10^5$, Nu can be related to $\mathrm{Pe_t}$ (Eq. 4) and Re as:

$$\mathrm{Nu} = 1 + (1 + \mathrm{Pe_t})^{1/3}\left(1 + \frac{0.096\mathrm{Re}^{1/3}}{1 + 7\mathrm{Re}^{-2}}\right) \tag{28}$$

With the above relations, the melting or dissociation rate can be calculated as follows. For a rising crystal of radius a, Eqs. 1, 19 and 20 are used to solve for u, Re and C_D simultaneously as long as Re is $\le 3\times 10^5$. Then $\mathrm{Pe_t}$ can be calculated from Eq. 4. Then Nu can be calculated from Eq. 28. Then δ_t can be calculated from $2a/\mathrm{Nu}$ (Eq. 27). Finally the melting rate can be calculated from Eq. 24.

By comparing the dissolution and dissociation rates (Eqs. 12 and 24), the ratio of dissociation rate to dissolution rate is:

$$\frac{(\mathrm{d}a/\mathrm{d}t)_{\mathrm{dissociation}}}{(\mathrm{d}a/\mathrm{d}t)_{\mathrm{dissolution}}} = \frac{\kappa}{D}\frac{\beta_t}{\beta_c}\frac{\delta_c}{\delta_t} \tag{29}$$

where $\kappa/D = \mathrm{Le} \approx 100$ where Le is the Lewis number. Mainly due to the large κ/D ratio, the dissociation rate is usually much greater than the dissolution rate.

5. Dissolution and dissociation of methane hydrate as it rises through seawater

The primary motivation of this study is to

understand methane hydrate dissolution and dissociation under various conditions although the above theories are general. In the following treatment, a piece of hydrate is assumed to behave as a perfect crystal. That is, the effects of grain boundaries, bubbles and other inclusions, cracks, and other defects of hydrate on dissolutions rates are ignored. The necessary parameters needed for calculation are summarized in Appendix 1[1]. Below, we consider dissolution of exposed hydrate floor, dissolution of a rising hydrate, and dissociation of a rising hydrate. We do not consider the unlikely case of dissociation of an exposed hydrate floor. It is unlikely because if hydrate is inherently unstable on the ocean floor, it is also inherently unstable in sediment due to temperature increase in sediment.

5.1. Dissolution of exposed hydrate floor

An exposed hydrate floor may stay at the ocean floor (that is, not rising through seawater) due to cohesion with sediment underneath or due to mixing of hydrate with sediment so that the overall density of hydrate and sediment is greater than that of seawater. In this section, we estimate the dissolution rates of such an exposed hydrate floor. The value of β_c (Eq. 8) does not change much with water depth (Table A1[1]). For a deep ocean floor temperature of 277.15 K, $\beta_c = 0.0094$, and D for methane in water is roughly 1.09×10^{-9} m^2/s (Appendix 1[1]). The value of α can be solved from Eq. 7 to be 0.0053. From Eq. 6, the diffusive dissolution distance X_{dis} (in m) is $3.5\times10^{-7}\sqrt{t}$ (where t is in s), 0.10 mm in a day, 2.0 mm in a year, and 2 m in a million years. That is, diffusive dissolution is extremely slow.

The above dissolution rates are a minimum because dissolution of massive methane hydrate on the ocean floor is aided by convection, either free convection driven by the density difference between methane-bearing interface seawater and normal seawater, or forced convection due to oceanic current. Kerr [11] modeled floor dissolution controlled by free convection. Compared to far-field seawater, the boundary layer above a hydrate floor is slightly colder (which makes it more dense), and contains slightly higher CH_4 content (which makes it less dense). As estimated by Kerr (personal communication), the thermal effect that stabilizes the boundary layer is greater than the compositional effect. Hence there would be no free convection.

Hydrate floor dissolution rate under forced convection due to oceanic current can be estimated using Eq. 10. For hydrate floor exposed at Hydrate Ridge (44.57°N, 125.19°W), ocean current velocity u is about 0.03 m/s (David Rea, personal communication), seawater viscosity at 277.15 K is about 0.00167 Pa s, the length scale l is roughly taken as 1000 m (the dependence of dissolution on the length scale l is weak). Hence the calculated dissolution rate V is 0.00228 μm/s, or 0.072 m per year. A 100 m thick massive hydrate layer may survive for more than 1000 years.

5.2. Convective dissolution of methane hydrate upon free ascent

We now calculate convective dissolution rate as methane hydrate rises buoyantly through seawater. Because the saturation concentration of CH_4 in water is low (Fig. 2), dissolved CH_4 is not expected to significantly affect the density, diffusivity and viscosity in the boundary layer. Hence we expect the theoretical calculation to have better accuracy than the case for NaCl and KBr descent and dissolution (Fig. 5). Since dissolution only occurs in deep water (dissociation occurs in shallow water) where temperature is roughly constant, for simplicity, a constant temperature of 277.15 K for deep water with a constant value of β_c (0.0094) is used.

Fig. 6 shows some calculated results. The ascent velocity of methane hydrate increases with its size. The calculated ascent velocity of a hydrate with 50 mm radius is 0.53 m/s. Brewer et al. [24] observed the ascent velocity of natural hydrate of similar size to be 0.24 m/s. The difference is probably due to: (i) impurity in natural hydrate that increases its density, (ii) difficulty in determining the size, and (iii) non-spherical shape of natural hydrate.

The dissolution rate decreases with increasing effective radius of the crystal (a). The dissolution

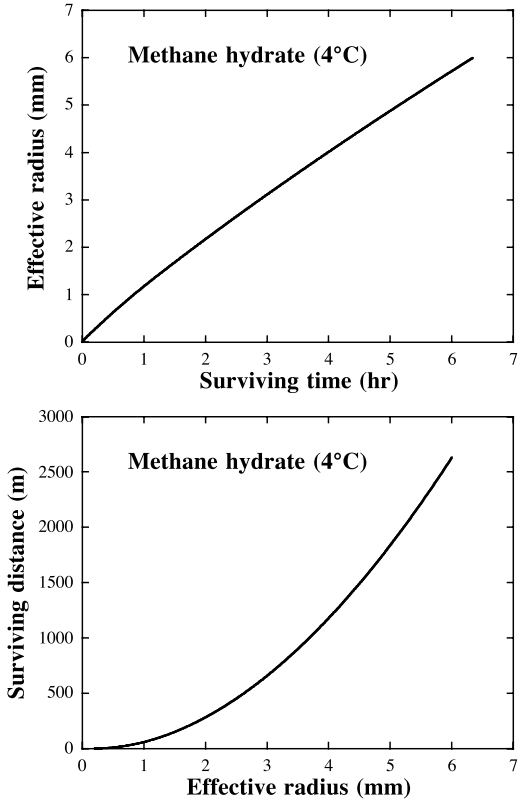

Fig. 6. Calculated relation between effective radius and surviving time, and between effective radius and surviving distance for methane hydrate dissolution and ascent in seawater.

rate is 0.16 μm/s for $a = 50$ mm, 0.24 μm/s for $a = 5$ mm, and 0.30 μm/s for $a = 1$ mm. Brewer et al. [24] used variation in the ascent velocity to estimate the variation in the size of hydrate, and obtained a dissolution rate of 31 μm/s, about two orders of magnitude greater than our results. This clearly shows that hydrate size cannot be estimated from ascent velocity. (Furthermore, there is an error in their eq. 1.) In another part of their paper [24], they argued that the dissolution rate is less than 6.7 μm/s, consistent with our calculation. The inconsistency between the two parts of their paper is not explained [24] but they have another submitted manuscript on the topic (Brewer, personal communication).

A larger hydrate piece rises more rapidly but dissolves more slowly. Hence per unit depth, dissolution distance is smaller for larger hydrate pieces. For the oceanic depth corresponding to Fig. 2, a piece of hydrate with radius greater than 5.5 mm would be able to survive the rise and dissolution from the ocean floor (2775 m) to reach the depth of 530 m where hydrate begins to dissociate. Solid curves in Fig. 7 show the size variation with depth for methane hydrate dissolution. As will be seen later, because hydrate dissociates in shallow seawater and the dissociation rate is much greater, only very large chunks of hydrate can survive dissociation and float to ocean surface.

Many hydrate grains may be released in a parcel of water. In this case the collective rise of hydrate-laden water must be considered. For example, consider a parcel of water 10 m in radius and containing 1 vol% of roughly uniformly distributed methane hydrate, lowering its density by 0.1% relative. The rising velocity of the parcel obtained from iterations of Eqs. 1 and 20 and the numerical standard drag curve (C_D vs. Re) [22] (more general than Eq. 19) is 1.2 m/s. The parcel would rise by 2000 m in 0.47 h. Hydrate

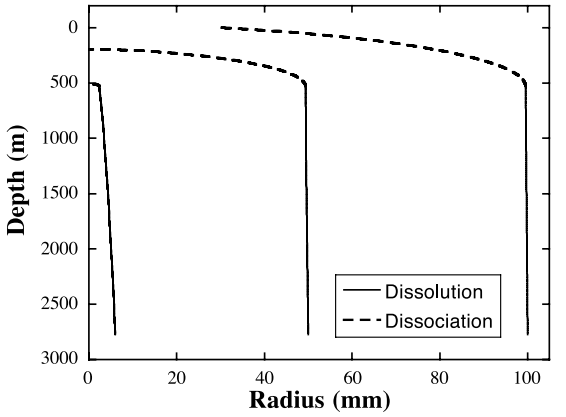

Fig. 7. Calculated hydrate size variation as a function of depth as hydrate rises and dissolves/dissociates through seawater. The initial depth is 2775 m (corresponding to Blake Ridge off North and South Carolina). There is dissolution between 2775 and 530 m depth, and dissociation at depth < 530 m (Fig. 2). Three cases are shown for different initial radii: 6 mm, 50 mm, and 100 mm. Starting from 2775 m depth, the time to ascent to 530 m depth is 4.19 h for $a_0 = 6$ mm, 1.18 h for $a_0 = 50$ mm, and 0.84 h for $a_0 = 100$ mm; the time to be completely dissolved is 4.27 h for $a_0 = 6$ mm, and 1.39 h for $a_0 = 50$ mm; and the time to reach surface for $a_0 = 100$ mm is 1.07 h.

with radius greater than 0.5 mm would be able to survive such a rise. As hydrate reaches shallow depth, it becomes unstable and dissociates, which is discussed next.

5.3. Convective dissociation of methane hydrate upon free ascent

Using the theory in Section 4, methane hydrate dissociation rate can be calculated numerically. During methane hydrate dissociation, bubbles are produced at the dissociation interface. Buoyant rise of bubbles would intensify convection and hence increase the dissolution rate, but the effect is difficult to quantify. Hence the calculation using our theory only gives a minimum of the dissociation rate.

Before modeling the full process of ascent and dissociation, we first compare dissociation and dissolution rates. If $\Delta T = T_\infty - T_0 = 1$ K in Eq. 25, using the relevant parameters, the dissociation rate is about 30 times the dissolution rate (Eq. 29). If $\Delta T = 10$ K, then the dissociation rate is about 300 times the dissolution rate (Eq. 29). The conclusion is that the dissociation rate is much greater than the dissolution rate as long as ΔT is large enough, consistent with expectations.

Methane hydrate dissociation as it rises through seawater would begin when water pressure is smaller than the pressure to stabilize hydrate, which is equivalent to when water temperature is higher than the dissociation temperature of hydrate. Dissociation would begin when $T_\infty - T_0$ (Eq. 25) begins to exceed zero. Therefore, our numerical modeling starts with a hydrate at the depth of 530 m (the boundary between water+gas and water+hydrate in Fig. 2) where $T_\infty - T_0 = 0$ and a water temperature of 279.36 K. As hydrate rises, water temperature T_∞ increases, and the pressure decreases so that the dissociation temperature T_0 decreases. The combined effect is that the difference $T_\infty - T_0$ increases and hydrate dissociation rate increases (Eqs. 24 and 25). In the model, T_0 is calculated from the pressure (depth), and T_∞ is calculated by assuming it increases linearly upward with a gradient of 0.03 K/m so that the surface temperature is 295.15 K. After a rise of about 0.6 m (from the starting point of 530 m), ΔT increases to 0.033 K and the dissociation rate equals the dissolution rate. With further rise of hydrate, dissociation rate becomes greater and greater. Fig. 7 (dashed curve) shows some calculated results for hydrate dissociation in the surface water. Methane hydrate with an effective radius of 5 mm would dissociate completely in 370 s and with a survival distance of only 47 m. To survive the whole 530 m column, the hydrate sphere must have an initial radius of 0.09 m or more. Because bubbles produced during dissociation intensify convection and hence dissociation rate, and because large chunks of hydrate likely have grain boundaries and pores (hence not behaving as a single perfect crystal), to survive the surface layer would require larger hydrate pieces.

Brewer et al. [24] observed that at Hydrate Ridge, pieces of hydrate with 0.04–0.05 m radius can survive a 410 m surface column. Because the hydrate is not pure methane hydrate, there is not enough information to do the calculation. However, because the depth is shallower than our calculation above, and the temperature in surface water is only 287 K [25] leading to a temperature gradient of 0.02 K/m (smaller than 0.03 K/m we used above), a simple scaling of our calculated result roughly agrees with Brewer et al.'s observed result. Although temperature profiles in surface ocean vary with location, there is always a surface seawater layer where methane hydrate is unstable with respect to dissociation. Hence only large hydrate chunks (greater than about 50 mm radius depending on the local temperature profile) would be able to survive dissociation through this layer and reach the surface. Smaller hydrate grains and pieces would rapidly dissociate into bubbles and water. Hence if many methane hydrate grains (1–10 mm in radius) are released into ocean bottom water, many (depending on whether they rise individually or collectively) would likely survive dissolution in deep water, especially if the hydrate-bearing water parcel rises collectively. Upon reaching inherent instability depth, hydrate would dissociate rapidly into methane gas and water in shallow water, producing a bubble plume, which might power a methane-driven oceanic eruption [4]. This would be an efficient way to transport

a large amount of CH_4 gas rapidly to the atmosphere.

6. References cited in the Appendices

[26,29–31]

Acknowledgements

We thank Bruce Buffet and Ross C. Kerr for constructive and insightful comments. Kerr also helped us to model floor dissolution rate under forced convection of ocean currents. We thank David Rea for helping with oceanography. Acknowledgment is made to the donors of the American Chemical Society Petroleum Research Fund for support of this research. This work is also partially supported by the US National Science Foundation (EAR-0125506 and EAR-0228752).*[KF]*

References

[1] E.D. Sloan, Clathrate Hydrates of Natural Gases, Marcel Dekker, New York, 1990, 641 pp.
[2] K.A. Kvenvolden, A primer on the geological occurrence of gas hydrate, in: J.P. Henriet, J. Mienert (Eds.), Gas Hydrate: Relevance to World Margin Stability and Climatic Change, Geol. Soc. London Spec. Publ. 137 (1998) 9–30.
[3] B.A. Buffett, Clathrate hydrates, Annu. Rev. Earth Planet. Sci. 28 (2000) 477–507.
[4] Y. Zhang, Methane-driven oceanic eruptions, Geophys. Res. Lett. 30 (2003) 51-1 to 51-4, 10.1029/2002GL016658.
[5] G.D. Spence, N.R. Chapman, R.D. Hyndman, C. Cleary, Fishing trawler nets massive 'catch' of methane hydrates, EOS 82 (2001) 621–627.
[6] R.J. Kirkpatrick, Crystal growth from the melt: a review, Am. Mineral. 60 (1975) 798–814.
[7] R.J. Kirkpatrick, Kinetics of crystallization of igneous rocks, Rev. Mineral. 8 (1981) 321–389.
[8] D. Walker, W.S. Kiefer, Xenolith digestion in large magma bodies, J. Geophys. Res. 90 (1985) C585–C590.
[9] Y. Zhang, D. Walker, C.E. Lesher, Diffusive crystal dissolution, Contrib. Mineral. Petrol. 102 (1989) 492–513.
[10] R.C. Kerr, Melting driven by vigorous compositional convection, J. Fluid Mech. 280 (1994a) 255–285.
[11] R.C. Kerr, Dissolving driven by vigorous compositional convection, J. Fluid Mech. 280 (1994b) 287–302.
[12] R.C. Kerr, Convective crystal dissolution, Contrib. Mineral. Petrol. 121 (1995) 237–246.
[13] A.C. Lasaga, Kinetic Theory in the Earth Sciences, Princeton University Press, Princeton, NJ, 1998, 811 pp.
[14] Y. Zhang, Crystal growth, in: C.P. Marshall, R.W. Fairbridge (Eds.), Encyclopedia of Geochemistry, Kluwer, Dordrecht, 1999, pp. 120–123.
[15] R.C. Kerr, Mass transfer, in: C.P. Marshall, R.W. Fairbridge (Eds.), Encyclopedia of Geochemistry, Kluwer, Dordrecht, 1999, pp. 384–387.
[16] E.L. Cussler, Diffusion: Mass Transfer in Fluid Systems, Cambridge University Press, Cambridge, 1984, 525 pp.
[17] D.F. Barnes, J.E. Hobble, Rate of melting at the bottom of floating ice, USGS Prof. Pap. 400 (1960) B392–B394.
[18] H.S. Carslaw, J.C. Jaeger, Conduction of Heat in Solids, Clarendon, Oxford, 1959, 510 pp.
[19] J.P. Holman, Heat Transfer, McGraw-Hill, New York, 2002, 688 pp.
[20] P. McLeod, R.S.J. Sparks, The dynamics of xenolith assimilation, Contrib. Mineral. Petrol. 132 (1998) 21–33.
[21] V.G. Levich, Physicochemical Hydrodynamics, Prentice-Hall, Englewood Cliffs, NJ, 1962, 700 pp.
[22] R. Clift, J.R. Grace, M.E. Weber, Bubbles, Drops, and Particles, Academic Press, New York, 1978, 380 pp.
[23] D.L. Turcotte, G. Schubert, Geodynamics: Applications of Continuum Physics to Geological Problems, Wiley and Sons, New York, 1982, 450 pp.
[24] P.G. Brewer, C. Paull, E.T. Peltzer, W. Ussler, G. Rehder, G. Friederich, Measurements of the fate of gas hydrates during transit through the ocean water column, Geophys. Res. Lett. 29 (2002) 38-1–38-4.
[25] M.G. Gross, Oceanography: A View of the Earth, Prentice-Hall, Englewood Cliffs, NJ, 1982, 498 pp.
[26] D.M. Maharajh, J. Walkley, The temperature dependence of the diffusion coefficients of Ar, CO_2, CH_4, CH_4Cl, CH_3Br, and $CHCl_2F$ in water, Can. J. Chem. 51 (1973) 944–952.
[27] G.R. Dickens, M.S. Quinby-Hunt, Methane hydrate stability in seawater, Geophys. Res. Lett. 21 (1994) 2115–2118.
[28] Z. Duan, N. Moller, J. Greenberg, J.H. Weare, The prediction of methane solubility in natural waters to high ionic strength from 0 to 250°C and from 0 to 1600 bar, Geochim. Cosmochim. Acta 56 (1992) 1451–1460.
[29] R.C. Weast, M.J. Astle, W.H. WBeyer, CRC Handbook of Chemistry and Physics, CRC Press, Boca Raton, FL, 1983, 2303 pp.
[30] J.A. Dean, Lange's Handbook of Chemistry, McGraw-Hill, New York, 1985, 1856 pp.
[31] C.J.D. Fell, H.P. Hutchison, Diffusion coefficients for sodium and potassium chlorides in water at elevated temperatures, J. Chem. Eng. Data 16 (1971) 427–429.
[32] G.R. Dickens, C.K. Paull, P. Wallace, the ODP Leg 164 Scientific Party, Direct measurement of in situ methane quantities in a large gas-hydrate reservoir, Nature 385 (1997) 426–428.